16. S. Mashchenko, H. M. P. Couchman, J. Wadsley, *Nature* **442**, 539 (2006).
17. F. I. Pelupessy, P. P. Papadopoulos, P. van der Werf, *Astrophys. J.* **645**, 1024 (2006).
18. A. Marcolini, A. D'Ercole, F. Brighenti, S. Recchi, *Mon. Not. R. Astron. Soc.* **371**, 643 (2006).
19. T. Abel, G. L. Bryan, M. L. Norman, *Science* **295**, 93 (2002).
20. N. Yoshida, T. Abel, L. Hernquist, N. Sugiyama, *Astrophys. J.* **592**, 645 (2003).
21. M. Ricotti, N. Y. Gnedin, *Astrophys. J.* **629**, 259 (2005).
22. J. I. Read, A. P. Pontzen, M. Viel, *Mon. Not. R. Astron. Soc.* **371**, 885 (2006).
23. J. W. Wadsley, J. Stadel, T. Quinn, *New Astron.* **9**, 137 (2004).
24. G. Stinson *et al.*, *Mon. Not. R. Astron. Soc.* **373**, 1074 (2006).
25. Materials and methods are available as supporting material on *Science* Online.
26. A. El-Zant, I. Shlosman, Y. Hoffman, *Astrophys. J.* **560**, 636 (2001).
27. C. Tonini, A. Lapi, P. Salucci, *Astrophys. J.* **649**, 591 (2006).
28. L. Mayer, S. Kazantzidis, C. Mastropietro, J. Wadsley, *Nature* **445**, 738 (2007).
29. S. Kazantzidis, A. R. Zentner, A. V. Kravtsov, *Astrophys. J.* **641**, 647 (2006).
30. J. M. Lotz *et al.*, *Astrophys. J.* **552**, 572 (2001).
31. The simulations reported in this paper were carried out on facilities of the Shared Hierarchical Academic Research Computing Network [(SHARCNET) www.sharcnet.ca]. The authors acknowledge the support of the Canadian Institute for Advanced Research, Natural Sciences and Engineering Research Council of Canada, and SHARCNET. To produce Fig. 1 and movie S1, we used the public domain program IFrIT written by N. Gnedin (Fermilab).

Supporting Online Material

www.sciencemag.org/cgi/content/full/1148666/DC1
Materials and Methods
Figs. S1 to S5
References
Movie S1

1 August 2007; accepted 9 November 2007
Published online 29 November 2007;
10.1126/science.1148666
Include this information when citing this paper.

Superconducting Vortices in $CeCoIn_5$: Toward the Pauli-Limiting Field

Andrea D. Bianchi,[1]*† Michel Kenzelmann,[2,3] Lisa DeBeer-Schmitt,[4] Jon S. White,[5] Edward M. Forgan,[5] Joel Mesot,[3] Markus Zolliker,[6] Joachim Kohlbrecher,[3] Roman Movshovich,[7] Eric. D. Bauer,[7] John L. Sarrao,[7] Zachary Fisk,[1] Cedomir Petrović,[8] Morten Ring Eskildsen[4]

Many superconducting materials allow the penetration of magnetic fields in a mixed state in which the superfluid is threaded by a regular lattice of Abrikosov vortices, each carrying one quantum of magnetic flux. The phenomenological Ginzburg-Landau theory, based on the concept of characteristic length scales, has generally provided a good description of the Abrikosov vortex lattice state. We conducted neutron-scattering measurements of the vortex lattice form factor in the heavy-fermion superconductor cerium-cobalt-indium ($CeCoIn_5$) and found that this form factor increases with increasing field—opposite to the expectations within the Abrikosov-Ginzburg-Landau paradigm. We propose that the anomalous field dependence of the form factor arises from Pauli paramagnetic effects around the vortex cores and from the proximity of the superconducting state to a quantum critical point.

$CeCoIn_5$ is a d-wave, heavy-fermion superconductor with a critical temperature T_c = 2.3 K (*1*). The interaction of Ce with the conduction electrons leads to an enhancement of the effective electron mass by several orders of magnitude. The competition between an instability toward antiferromagnetic ordering (suppressed by superconductivity) and a paramagnetic state leads to a quantum critical point at the upper critical field, H_{c2}, and an associated non–Fermi liquid behavior (*2*, *3*). The heavy electron mass (and, for the field parallel to the planes, the 2d electronic structure) suppresses orbiting supercurrents circling the vortices. Hence, the upper critical field at low temperature in $CeCoIn_5$ is not determined by the usual orbital depairing. Instead, it is limited by the Pauli spin susceptibility of the electrons, which favor the electron spins to line up parallel to a magnetic field, which is in competition with the antiparallel alignment required for Cooper pairing in a singlet superconductor (*4*). In $CeCoIn_5$, the Pauli-limiting field is smaller than the orbital upper critical field H_{c2}^{orb} by a factor of >2.5, as extrapolated from measurements near T_c (*5*), and the transition to the normal state at low temperatures becomes first-order (*5*, *6*). Finally, $CeCoIn_5$ can be prepared as an ultraclean superconductor with an electron mean free path (ℓ) of several micrometers, three orders of magnitude larger than the superconducting coherence length (*7*, *8*).

The Ginzburg-Landau (GL) model is a phenomenological description of a superconducting phase with only two parameters: the coherence length ξ of the superconducting order parameter, and the penetration depth λ of magnetic fields into the superconducting phase. Abrikosov showed that the GL model describes the mixed state of type II superconductors (*9*), where quantum flux tubes with a core size of $\sim\xi$ penetrate the superconductor in a regular vortex lattice (VL). The Abrikosov-Ginzburg-Landau (AGL) picture gives a good description of the mixed-state properties of orbitally limited superconductors, but it is not known to what extent the AGL model applies for Pauli-limited superconductors, particularly close to the upper critical field.

One of the predicted scenarios for the superconducting Cooper pairs in Pauli-limited superconductors at high fields is that they are no longer formed by a pairing of spin-up and spin-down electrons carrying opposite momenta; instead, the superconducting order parameter carries a finite momentum, giving rise to an inhomogeneous superconducting state known as the Fulde-Ferrell-Larkin-Ovchinnikov (FFLO) state (*10*, *11*). In the Larkin-Ovchinnikov form of such a state, the superconducting order parameter is expected to develop regularly spaced planar nodes perpendicular to the vortex lines (*12*). A number of experiments on $CeCoIn_5$ provide evidence for a phase transition inside the superconducting state near H_{c2} consistent with a FFLO state (*12*). Although the majority of these measurements were performed with the field parallel to the basal plane of the tetragonal unit cell, the possible existence of an FFLO state has also been reported for an applied field along the *c* axis (*12*–*14*).

In our experiment, the VL was imaged by small-angle neutron scattering (SANS), using the direct coupling of the magnetic moment of the neutron to the spatial variation of the magnetic field created by the VL (*15*). Figure 1 shows the evolution of the VL diffraction patterns with increasing magnetic field at 50 mK. The VL in real space has the same symmetry as its diffraction pattern but is rotated by 90° about the field axis. At the lowest fields, the VL of $CeCoIn_5$ has a distorted hexagonal symmetry, giving two equivalent domain orientations and hence 2×6 first-order reflections, which are symmetric with respect to the [110] crystallographic direction (Fig. 1, A and D). With increasing field, the VL undergoes a first-order transition at H_1 = 0.55 T to a rhombic symmetry indicated by 2×4 Bragg reflections (Fig. 1, B and E). Upon further increasing the field, the VL continuously transforms into an ideal, single-domain square symmetry (Fig. 1, C and F) at H_2 = 1.1 T. This evolution of the VL symmetry is in agreement with our earlier studies conducted in fields up to 2 T (*16*, *17*). At higher fields, this sequence of phase transitions reverses (Fig. 1, G and H), with the VL undergoing a transition to a rhombic

[1]Department of Physics and Astronomy, University of California, Irvine, CA 92697, USA. [2]Laboratory for Solid State Physics, ETH Zürich, CH-8093 Zürich, Switzerland. [3]Laboratory for Neutron Scattering, ETH Zürich and Paul Scherrer Institute, CH-5232 Villigen PSI, Switzerland. [4]Department of Physics, University of Notre Dame, Notre Dame, IN 46556, USA. [5]School of Physics and Astronomy, University of Birmingham, Birmingham B15 2TT, UK. [6]Laboratory for Developments and Methods, Paul Scherrer Institute, CH-5232 Villigen PSI, Switzerland. [7]MPA-10, Los Alamos National Laboratory, Los Alamos, NM 87545, USA. [8]Condensed Matter Physics and Materials Science Department, Brookhaven National Laboratory, Upton, NY 11973, USA.

*Present address: Département de Physique, Université de Montréal, Montréal, Quebec H3C 3J7, Canada.
†To whom correspondence should be addressed. E-mail: andrea.bianchi@umontreal.ca

(at $H_2' = 3.4$ T) and finally a distorted hexagonal symmetry (at $H_3 = 4.4$ T).

Further measurements taken at higher temperatures establish the field-temperature VL structural phase diagram (Fig. 2). We note that the phase boundary of the high-field "hexagonal" phase does not intersect with the onset of the first-order nature of H_{c2} (*5*), nor does it coincide with the proposed FFLO phase boundary (*12*, *14*). At higher temperatures, where thermal excitation reduces the effects of anisotropy, fewer VL phases are observed. We also note that the sequence of VL phase transitions is qualitatively similar to that in $TmNi_2B_2C$ (*18*), where localized-moment antiferromagnetic order interacts with the superconducting order parameter. Both compounds have a strong paramagnetic response, which suggests that this may be the driving force leading to the sequence of phase transitions. However, unlike $TmNi_2B_2C$, which has well-ordered local moments, in $CeCoIn_5$ superconductivity is thought to supersede magnetism (*2*).

The VL structural transitions in Fig. 2 at low field and temperature may be understood in the following terms: In the limit of large distances, the vortex lines are isotropic around the screening current plane, as this is the tetragonal crystal basal plane. As the field is increased and the vortices move closer together, there are two effects that can lead to the hexagonal-rhombic-square sequence of transitions: (i) d-wave effects (*19*, *20*), and (ii) the nonlocal relation between supercurrent density **j** and vector potential **A** due to a finite coherence length (*21*). If the square VL is due to d-wave effects, then the nearest neighbors should be aligned along the nodal directions of the d-wave order parameter (*22*), consistent with the $d_{x^2-y^2}$ pairing reported for $CeCoIn_5$ (*23*).

More surprising is the reversal of the sequence of phase transitions, back to a nearly isotropic hexagonal VL, as the field approaches H_{c2} (which is a region not accessible in the d-wave high-T_c superconductors). A reentrant square VL phase has been predicted theoretically, attributed to opposing anisotropies of the Fermi surface and the energy gap (*24*) or to strong fluctuations near H_{c2} (*25*). However, neither of these theories is clearly applicable to $CeCoIn_5$. We propose instead that a quite different mechanism becomes important when the vortex spacing becomes comparable to the core size. A qualitative explanation for the weakening of the fourfold anisotropy at high fields may lie in the observation that, by continuity, the field at the center of a vortex must exhibit cylindrical symmetry, just as it does at large distances; the "four-leaved clover" anisotropy is strong only at intermediate distances [see, e.g., (*26*)]. The proposed tendency toward isotropy at large fields is seen in free energy calculations (*20*), and this tendency may be amplified by the Pauli limiting process that becomes increasingly important near H_{c2}, with induced paramagnetic moments in the vortex cores that are less sensitive than the orbital supercurrents to the crystallographic directions.

We now analyze the diffracted intensity arising from the spatial variation of the magnetic field due to the VL. The total intensity of a diffraction peak, integrated over angle as the VL is rocked through the Bragg condition (*15*), is proportional to the square modulus of the VL form factor $F(\mathbf{q}_{hk})$, which is the Fourier transform at wave vector $\mathbf{q}_{hk}$ of the two-dimensional magnetic flux density of the VL. In the limit of very low fields, the London approach with negligible vortex core effects should apply, and $|F|^2$ depends only on λ with the value $[\sqrt{3}\phi_0/(8\pi^2\lambda^2)]^2$, where ϕ_0 is the flux quantum. Our measured $|F|^2$

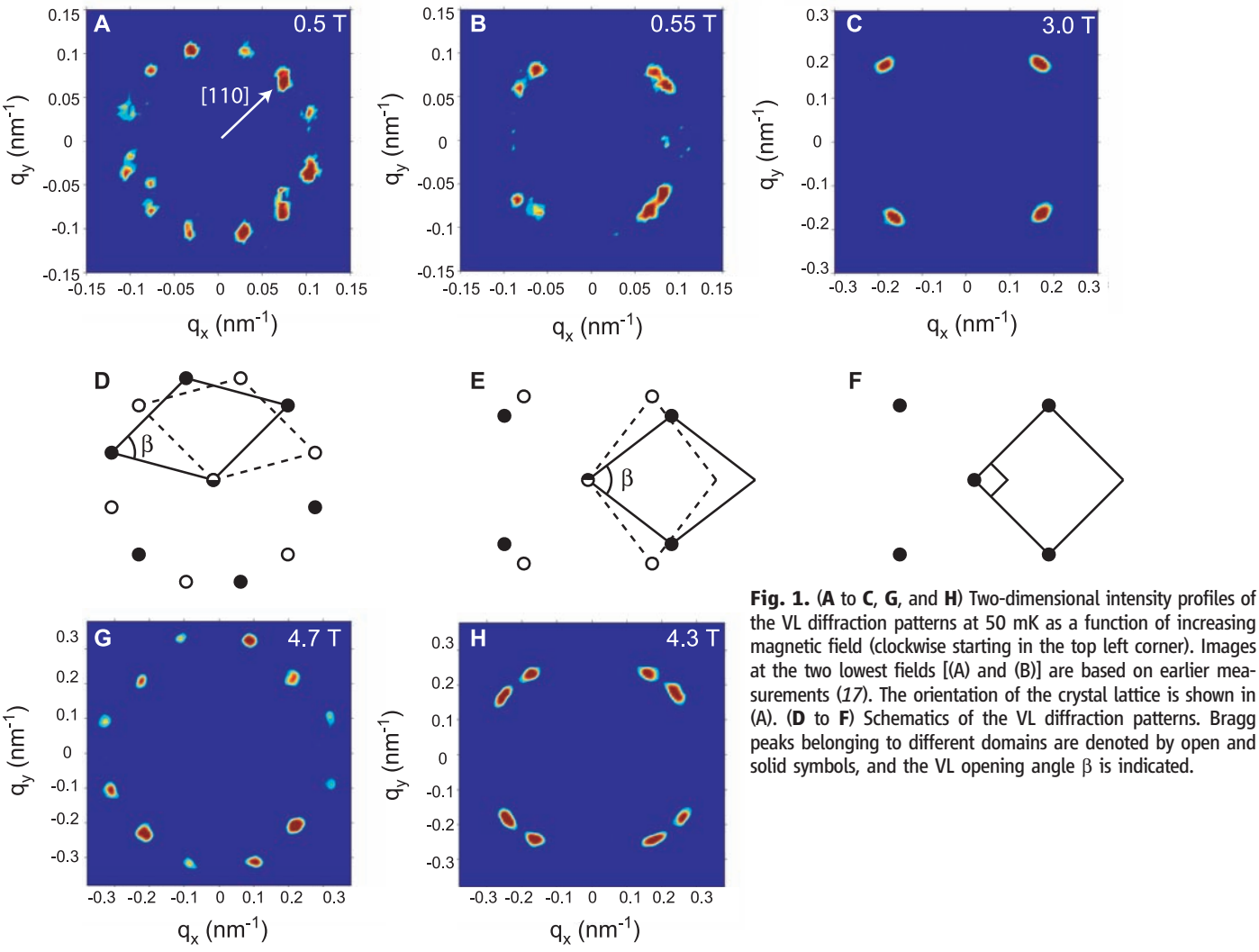

Fig. 1. (**A** to **C**, **G**, and **H**) Two-dimensional intensity profiles of the VL diffraction patterns at 50 mK as a function of increasing magnetic field (clockwise starting in the top left corner). Images at the two lowest fields [(A) and (B)] are based on earlier measurements (*17*). The orientation of the crystal lattice is shown in (A). (**D** to **F**) Schematics of the VL diffraction patterns. Bragg peaks belonging to different domains are denoted by open and solid symbols, and the VL opening angle β is indicated.

implies a value of $\lambda = 4650$ Å, about double the values obtained in zero field by other techniques (*27*, *28*); the cause of this difference is not clear at present. Since the early work on Nb (*29*), it has been observed that $|F|^2$ decreases monotonically as the vortices move closer together and their field distributions overlap. Both the GL model and numerical calculations predict an approximately exponential decrease of the form factor at low and intermediate fields for both s- and d-wave superconductors (*20*, *30*). Near H_{c2} Abrikosov's solution to the GL equations predicts that $|F|^2$ falls quadratically to zero (*31*). Figure 3 shows the measured form factor in $CeCoIn_5$ at $T = 50$ mK and 0.5 K, which is in striking contrast to typical AGL field dependence shown by the dashed lines. Below 2 T, $|F|^2$ is essentially constant, in agreement with previous reports (*17*), followed by a monotonic increase by a factor of ~4 with field up to 4.5 T at both 50 and 500 mK. An additional testimony to the increasing form factor is given by the fact that a strong VL diffraction pattern was observed even at 4.9 T (within 50 mT of H_{c2}).

The GL picture can be generalized by allowing the characteristic lengths to vary with field. This was the approach of earlier work, which, motivated by theoretical predictions for ultraclean superconductors (*32*), used a field-dependent core size ξ to explain the unexpected constancy of $|F|^2$ below 2 T (*17*). With the increase in $|F|^2$ reported here, however, a parameterization of our results between 0.5 and 4.5 T by a field-dependent ξ would require a decrease of the core size by a factor of more than 5. In comparison, previous experimental reports of core contraction show that it occurs mainly at low vortex densities (*33*), and although ξ decreases, the ratio of the core size to the vortex separation increases with field, causing $|F|^2$ to decrease. Within the Bardeen-Cooper-Schrieffer (BCS) and GL approach, the BCS coherence length ξ_0 is field-independent and $\xi_{GL} \propto \hbar v_F/k_B T_c$ (where $\hbar$ is the Planck constant divided by 2π, v_F is the Fermi velocity, and k_B is the Boltzmann constant). To explain our results strictly in such terms would require a large increase of the pairing interaction with field (which we regard as very unlikely) or would require a decrease in the Fermi velocity, which would entail an increase in λ and a decrease of $|F|^2$. We also exclude the possibility that an increase in $|F|^2$ could be explained by a decrease in λ, as this would imply a superfluid density increasing toward H_{c2}. Thus, our results present a clear departure from the AGL paradigm. This conclusion is also indirectly supported by observations of an unusual broadening of the nuclear magnetic resonance line shape in the mixed state of $CeCoIn_5$ [see (*12*), references 28 and 120].

Instead, we ascribe the increase in $|F|^2$ at large fields to a contribution of electron spin polarization to the magnetic induction in the vortex cores. A similar process has been studied in the borocarbide superconductor $TmNi_2B_2C$, which has localized magnetic moments (*34*).

In a strongly Pauli-limited superconductor, it is expected that parallel spin alignment of the quasi-particles would be greater in the cores, where the Cooper pairs are broken. This conclusion is strengthened by recent first-principles calculations, which indeed show an increase in $|F|^2$ with field arising from paramagnetic effects (*35*). However, there is not complete agreement, as an increasing form factor requires a ratio between the Pauli limiting field and the orbital limiting field, which is larger than the one found experimentally for $CeCoIn_5$. This discrepancy may arise from the fact that the magnetic susceptibility in the *c* direction is twice that for the basal plane (*6*), whereas the heat capacity in the normal state is approximately independent of field direction, suggesting an additional enhancement of paramagnetic effects for fields along the *c* axis. Alternatively, it may be the quantum critical point at $H_{c2}(T = 0)$ that leads to a divergence of the heavy fermion masses as measured by de Haas–van Alphen measurements (*36*) and heat capacity (*2*), possibly leading both to an enhancement of the paramagnetic effect and to a limitation of the vortex core size, both of which would tend to maintain a large form factor to high fields.

Finally, we draw attention to the drop in $|F|^2$ just below H_{c2} shown in our lowest-temperature data in Fig. 3. This drop does not coincide with a VL structure change. However, it does occur in the field and temperature region where other measurements have been interpreted as evidence for a FFLO phase with field direction parallel to the *c* axis (*12*–*14*). Certainly, the additional zeroes in the order parameter in a spatially modulated FFLO state would be expected to

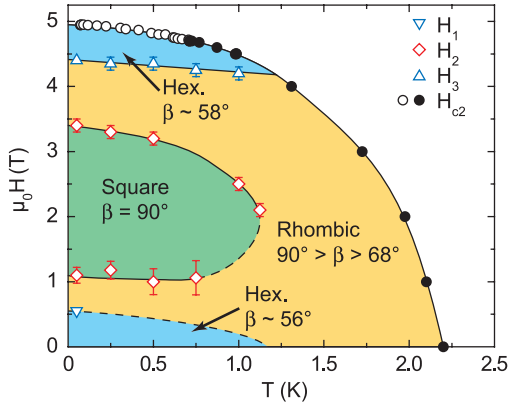

Fig. 2. Structural phase diagram for the VL in $CeCoIn_5$ with the magnetic field parallel to the *c* axis. The exact location of the hexagonal to rhombic transition H_1 was reliably determined only at base temperature, and the dashed line thus denotes our best estimate at higher temperatures. Likewise, there is some uncertainty in the lower branch of the square to rhombic transition H_2 between 0.75 and 1.25 K. The upper critical field is from (*5*). Above 0.7 K, H_{c2} is second order (solid circles). Below 0.7 K, the transition from the superconducting to the normal state becomes first order (open circles) because of the combination of high cleanliness and dominating Pauli paramagnetic limiting.

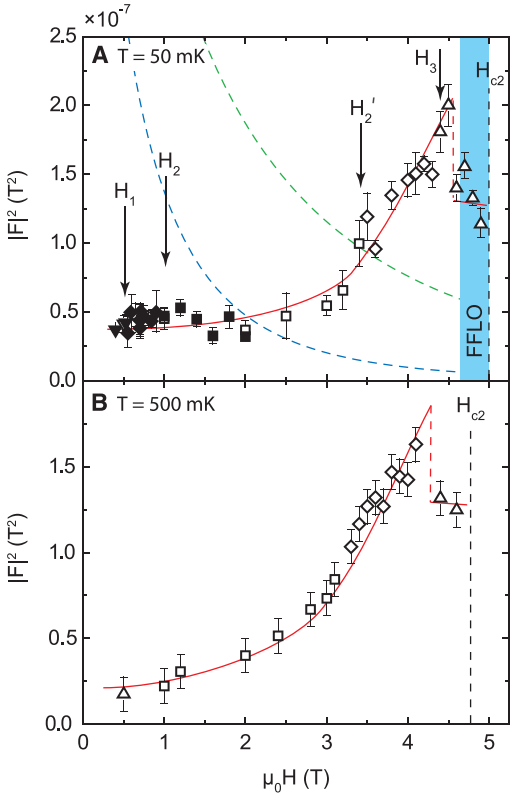

Fig. 3. Field dependence of the VL form factor for the (1,0) Bragg reflection at 50 mK (**A**) and 0.5 K (**B**). Solid symbols indicate earlier results obtained below 2 T (*17*). The lines through the data are guides to the eye. The VL symmetry transition fields H_1, H_2, and H_3 at 50 mK are indicated by arrows, and the upper critical field is shown by the vertical dashed lines. The green and blue dashed lines in the upper panel correspond to $|F|^2$ calculated from the Clem model (*30*) using a constant $\lambda = 235$ nm and $\xi_{c2} = 8.1$ nm (blue) or $\xi_{orb} = 5.0$ nm (green). The blue shaded region in the upper panel indicates the fields above which a FFLO phase has been reported on the basis of magnetization measurements (*14*).

reduce the form factor. Even without this indirect evidence for the predicted FFLO state, our main conclusion remains that in this strongly Pauli-limited superconductor with a quantum critical point at $H_{c2}(T = 0)$, the mixed state departs in many respects from the classical Abrikosov VL.

References and Notes

1. C. Petrović *et al.*, *J. Phys. Condens. Matter* **13**, L337 (2001).
2. A. Bianchi, R. Movshovich, I. Vekhter, P. G. Pagliuso, J. L. Sarrao, *Phys. Rev. Lett.* **91**, 257001 (2003).
3. M. A. Tanatar, J. Paglione, C. Petrović, L. Taillefer, *Science* **316**, 1320 (2007).
4. A. M. Clogston, *Phys. Rev. Lett.* **9**, 266 (1962).
5. A. Bianchi *et al.*, *Phys. Rev. Lett.* **89**, 137002 (2002).
6. T. Tayama *et al.*, *Phys. Rev. B* **65**, 180504 (2002).
7. R. Movshovich *et al.*, *Phys. Rev. Lett.* **86**, 5152 (2001).
8. Y. Kasahara *et al.*, *Phys. Rev. B* **72**, 214515 (2005).
9. A. A. Abrikosov, *Sov. Phys. JETP* **5**, 1174 (1957).
10. A. I. Larkin, Y. N. Ovchinnikov, *Sov. Phys. JETP* **20**, 762 (1965).
11. P. Fulde, R. A. Ferrell, *Phys. Rev. A* **550**, 135 (1964).
12. Y. Matsuda, H. Shimahara, *J. Phys. Soc. Jpn.* **76**, 051005 (2007), and references therein.
13. A. Bianchi, R. Movshovich, C. Capan, P. G. Pagliuso, J. L. Sarrao, *Phys. Rev. Lett.* **91**, 187004 (2003).
14. X. Gratens *et al.*, http://arxiv.org/abs/cond-mat/0608722 (2006).
15. See supporting material on *Science* Online.
16. M. R. Eskildsen, C. D. Dewhurst, B. W. Hoogenboom, C. Petrović, P. C. Canfield, *Phys. Rev. Lett.* **90**, 187001 (2003).
17. L. DeBeer-Schmitt, C. D. Dewhurst, B. W. Hoogenboom, C. Petrović, M. R. Eskildsen, *Phys. Rev. Lett.* **97**, 127001 (2006).
18. M. R. Eskildsen *et al.*, *Nature* **393**, 242 (1998).
19. M. H. S. Amin, I. Affleck, M. Franz, *Phys. Rev. B* **58**, 5848 (1998).
20. M. Ichioka, A. Hasegawa, K. Machida, *Phys. Rev. B* **59**, 8902 (1999).
21. V. G. Kogan *et al.*, *Phys. Rev. B* **55**, R8693 (1997).
22. S. P. Brown *et al.*, *Phys. Rev. Lett.* **92**, 067004 (2004).
23. A. Vorontsov, I. Vekhter, *Phys. Rev. Lett.* **96**, 237001 (2006).
24. N. Nakai, P. Miranović, M. Ichioka, K. Machida, *Phys. Rev. Lett.* **89**, 237004 (2002).
25. A. Gurevich, V. G. Kogan, *Phys. Rev. Lett.* **87**, 177009 (2001).
26. M. Franz, C. Kallin, P. I. Soininen, A. J. Berlinsky, A. L. Fetter, *Phys. Rev. B* **53**, 5795 (1996).
27. R. J. Ormeno, A. Sibley, C. E. Gough, S. Sebastian, I. R. Fisher, *Phys. Rev. Lett.* **88**, 047005 (2002).
28. S.Özcan *et al.*, *Europhys. Lett.* **62**, 412 (2003).
29. J. Schelten, H. Ullmaier, W. Schmatz, *Phys. Status Solidi B* **48**, 619 (1971).
30. J. R. Clem, *J. Low Temp. Phys.* **18**, 427 (1975).
31. E. M. Forgan *et al.*, *Phys. Rev. Lett.* **88**, 167003 (2002).
32. V. G. Kogan, N. V. Zhelezina, *Phys. Rev. B* **71**, 134505 (2005).
33. J. E. Sonier, *J. Phys. Condens. Matter* **16**, S4499 (2004).
34. L. DeBeer-Schmitt *et al.*, *Phys. Rev. Lett.* **99**, 167001 (2007).
35. M. Ichioka, K. Machida, *Phys. Rev. B* **76**, 064502 (2007).
36. R. Settai *et al.*, *J. Phys. Condens. Matter* **13**, L627 (2001).

37. This work is based on experiments performed at the Swiss spallation neutron source SINQ, Paul Scherrer Institute, Villigen, Switzerland. Supported by NSF grant NSF-DMR-0600742 (A.D.B. and Z.F.), the Alfred P. Sloan Foundation (M.R.E.), the European Commission under the 6th Framework Programme through the Key Action: Strengthening the European Research Area, Research Infrastructures (contract RII3-CT-2003-505925), the Swiss National Science Foundation (contract PP002-102831), the Swiss National Center of Competence in Research program "Materials with Novel Electronic Properties," the UK Engineering and Physical Sciences Research Council, and the U.S. Department of Energy, Office of Basic Energy Sciences. Part of this work was carried out at the Brookhaven National Laboratory, which is operated for the U.S. Department of Energy by Brookhaven Science Associates (DE-Ac02-98CH10886). We thank L. N. Bulaevskii, C. Capan, V. G. Kogan, K. Machida, and I. Vekhter for discussions during the preparation of the manuscript.

Supporting Online Material

www.sciencemag.org/cgi/content/full/319/5860/177/DC1
Materials and Methods
Fig. S1

17 September 2007; accepted 21 November 2007
10.1126/science.1150600

Self-Assembled Water-Soluble Nucleic Acid Probe Tiles for Label-Free RNA Hybridization Assays

Yonggang Ke,[1,3] Stuart Lindsay,[1,3,4] Yung Chang,[2,5] Yan Liu,[1,3] Hao Yan[1,3]*

The DNA origami method, in which long, single-stranded DNA segments are folded into shapes by short staple segments, was used to create nucleic acid probe tiles that are molecular analogs of macroscopic DNA chips. One hundred trillion probe tiles were fabricated in one step and bear pairs of 20-nucleotide-long single-stranded DNA segments that act as probe sequences. These tiles can hybridize to their targets in solution and, after adsorption onto mica surfaces, can be examined by atomic force microscopy in order to quantify binding events, because the probe segments greatly increase in stiffness upon hybridization. The nucleic acid probe tiles have been used to study position-dependent hybridization on the nanoscale and have also been used for label-free detection of RNA.

The detection of low levels of gene expression (*1*) has been enabled by technologies such as DNA microarrays (*2*, *3*) and reverse transcription polymerase chain reaction (RT-PCR) (*4*). Nonetheless, these technologies are still expensive (*5*), require probe labeling, and are hard to scale down to sample volumes comparable to those of single cells. Sample volumes have been reduced and sensitivities have been increased, but target detection still relies heavily on enzymatic manipulation and amplification to create detectable signals. We present an alternative that complements benchtop arrays in which individual self-assembled nucleic acid "tile" molecules, formed by "stapling" long, single-stranded DNA segments with shorter strands into shapes, can act as hybridization probes for molecules such as mRNAs in solution. After binding, the tiles can be adsorbed onto mica surfaces and are detected by atomic force microscopy (AFM). Thus, the probe tiles are reagents that are hybridized in solution and then titrated to quantify the targets.

Because the probes are placed on each nucleic acid tile with nanometer-scale precision, the effects of probe placement can be explored with molecular resolution. We found that the exact position of the probe made a substantial difference to hybridization efficiency. We circumvented this problem by manufacturing "bar-coded" tiles in which all of the probes were placed in an optimal position, and each type of nucleic acid tile was distinguished with a distinctive code represented by a group of dumbbell-shaped DNA loops protruding out of the tile surface as topographic registration markers; each coded tile detected one gene product.

Our ability to detect single-molecule hybridization with AFM appears to be enabled by the difference in the elastic properties of single- and double-stranded DNA or of the RNA-DNA hybrid. Detection sensitivity was, in this case, limited only by nucleic acid tile concentration down to the 200 pM levels, which we were able to image readily.

The design of the nucleic acid probe tiles and the read-out mechanism for the target binding are illustrated in Fig. 1. The foundation of the tile design was based on "scaffolded DNA origami" (Fig. 1A): a self-assembling technique for one-step synthesis of fully addressable DNA nanostructures (*6*). Rothemund (*6*) demonstrated that a long, single-stranded viral DNA scaffold can be folded and stapled by a large number of short synthetic "helper strands" into nanostructures that display complex patterns. A one-step nanomolar-scale synthesis yields $>10^{14}$ origami tiles with nearly 100% yield.

We used a simple, rectangular-shaped design, and its layout is shown schematically in Fig. 1A. Three different sequences of capture probes were included on the origami tile, corresponding to a region of three genes—*Rag-1*, *c-myc*,

[1]Center for Single Molecule Biophysics, Arizona State University, Tempe, AZ 85287, USA. [2]Center for Infectious Diseases and Vaccinology, The Biodesign Institute, Arizona State University, Tempe, AZ 85287, USA. [3]Department of Chemistry and Biochemistry, Arizona State University, Tempe, AZ 85287, USA. [4]Department of Physics, Arizona State University, Tempe, AZ 85287, USA. [5]School of Life Sciences, Arizona State University, Tempe, AZ 85287, USA.

*To whom correspondence should be addressed. E-mail: hao.yan@asu.edu

Superconducting Vortices in $CeCoIn_5$: Toward the Pauli-Limiting Field

Andrea D. Bianchi *et al.*

Science **319**, 177 (2008);
DOI: 10.1126/science.1150600